Title

Simulating Energy Relaxation in Pump–Probe Vibrational Spectroscopy of Hydrogen-Bonded Liquids

Journal

Journal of Chemical Theory and Computation, 13(3)

ISSN

1549-9618

Authors

Dettori, Riccardo
Ceriotti, Michele
Hunger, Johannes
et al.

Publication Date

2017-03-14

DOI

10.1021/acs.jctc.6b01108

Peer reviewed

Simulating energy relaxation in pump-probe vibrational spectroscopy of hydrogen-bonded liquids

Riccardo Dettori,[†] Michele Ceriotti,[‡] Johannes Hunger,[¶] Claudio Melis,[†] Luciano Colombo,[†] and Davide Donadio[*,§]

[†]*Dipartimento di Fisica, Università di Cagliari, Cittadella Universitaria, I-09042 Monserrato (CA), Italy*

[‡]*Laboratory of Computational Science and Modeling, IMX, École Polytechnique Fédérale de Lausanne, 1015 Lausanne, Switzerland*

[¶]*Max Planck Institute for Polymer research, Ackermannweg 10, 55128 Mainz, Germany*

[§]*Department of Chemistry, University of California Davis, One Shields Avenue, Davis, California 95616, United States*

E-mail: ddonadio@ucdavis.edu

Abstract

We introduce a non-equilibrium molecular dynamics simulation approach, based on the generalized Langevin equation, to study vibrational energy relaxation in pump-probe spectroscopy. A colored noise thermostat is used to selectively excite a set of vibrational modes, leaving the other modes nearly unperturbed, to mimic the effect of a monochromatic laser pump. Energy relaxation is probed by analyzing the evolution of the system after excitation in the microcanonical ensemble, thus providing direct information about the energy redistribution paths at the molecular level and their time scale. The method is applied to hydrogen bonded

molecular liquids, specifically deuterated methanol and water, providing a robust picture of energy relaxation at the molecular scale.

1 Introduction

Vibrational spectroscopy, in particular time-resolved pump-probe infrared spectroscopy, is a powerful tool to investigate the dynamics of molecular systems. In particular, hydrogen bonded liquids are among the most studied systems, as they exhibit intricate energy dissipation dynamics due to the strong directionality of hydrogen bonds and the complex topology of their network.[1,2]

Hydrogen bond interaction can be probed in detail by exploiting the stretching mode frequency of specific functional groups, for example the hydroxyl groups in liquid alcohols or water.[3–6] Time-resolved one-dimensional nonlinear spectroscopy is based on a pair of laser pulses, which are used to excite the sample, inducing a change in infrared absorption, and to probe the time dependent optical response. Time-resolved dynamical information is obtained by probing the evolution of an excited vibrational state as a function of delay time. Such dynamics are dominated by the dissipation of vibrational energy and by spectral diffusion. Both effects result from anharmonicity and from coupling among vibrational modes. The corresponding molecular transitions probed during the excitation and relaxation processes involve excited states, where the stretching mode is coupled with lower frequency modes via hydrogen bonding, causing spectral diffusion and non-trivial changes in spectral line shapes and width.[7–10] Furthermore, polarized infrared spectroscopy makes it possible to study the rotational dynamics of such molecules.[11–13]

To obtain the underlying molecular-level details of pump probe experiments, vibrational relaxation dynamics has been extensively investigated in computer simulations and several approaches have been proposed. On the one hand, equilibrium simulations have helped in the study of rotational dynamics, by means of autocorrelation functions using the fluctuation-dissipation formalism.[14,15] On the other hand, non-equilibrium simulations have been already adopted in relaxation processes, providing physical insight on the origin of spectral diffusion in the ultra-fast dynamics

of water[16–21].

However, the non-equilibrium approaches proposed so far either were designed *ad hoc* for a specific system,[16] or introduced an explicit oscillating electric field potential in the the Hamiltonian, the implementation of which poses fundamental and technical issues in systems with periodic boundary conditions.[22]

In this work we propose a general approach based on the Generalized Langevin Equation (GLE) to simulate pump-probe processes in non-equilibrium molecular dynamics simulations. This approach consists of using a non-Markovian thermostat that couples to the excited vibrational mode (pump), while the rest of the system remains at the equilibrium temperature. When the thermostat is switched off, the system relaxes to equilibrium, redistributing the excess energy among the other degrees of freedom. Such transient regime is monitored (probe) providing quantitative insight into relaxation energy transfer processes at the molecular scale. The method proposed, based on classical molecular dynamics, lacks the possibility of directly simulating quantum phenomena, but it can still be connected to vibrational energy relaxation rates,[23] and it is suitable to simulate long-time thermal relaxation.

The paper is organized as follows: first a brief and general introduction on the GLE is given, focusing on the frequency dependent coupling between the thermostat and the system; then a first case study, namely liquid methanol, is presented together with a detailed systematic analysis of technical aspects of the thermostat; finally, we report a second application on liquid water in order to highlight the portability of the method and the physical differences between the two systems.

2 Generalized Langevin Thermostat

To prepare the system in an out-of-equilibrium configuration where just few selected vibrational modes are excited, we make use of the Generalized Langevin Thermostat formalism. Although details on this approach and its implementation can be found elsewhere,[24,25] for the sake of completeness we summarize briefly its main features.

The Langevin equations that describe the Brownian motion of a particle with position x and momentum p, subject to a potential $V(x)$, can be written as:

$$\begin{aligned} \dot{x} &= p(t)/m \\ \dot{p} &= -V'(x) - \gamma p + \sqrt{2m\gamma/\beta}\xi(t) \end{aligned} \tag{1}$$

where $\beta = 1/k_B T$ is the inverse temperature, while the friction coefficient γ determines the interaction between the system and the Langevin heat bath and the fluctuations of the total energy. $\xi(t)$ is a Gaussian-distributed random force, delta-correlated, $\langle \xi(t)\xi(0) \rangle = \delta(t)$, and with zero mean, $\langle \xi \rangle = 0$. The delta-correlation of the stochastic forces implies that past events have no influence on the present state of the system, i.e. the dynamics is Markovian .

The Fourier transform of the delta-correlated random force is a flat profile in the frequency domain. Thus, coupling the system with a thermostat governed by the Langevin equation results in thermalization that affects the whole vibrational spectrum. For our purposes, it is necessary to introduce a spectrally resolved thermostat. To this end, the Markovian Langevin Equation (Eq.(1)) can be generalized by introducing history dependent terms:[26]

$$\begin{aligned} \dot{x} &= p(t)/m \\ \dot{p} &= -V'(x) - \int_{-\infty}^{t} K(t-s)p(s)ds + \zeta(t) \end{aligned} \tag{2}$$

where the friction coefficient was replaced by an integral over time of the momentum weighted by a memory kernel $K(t)$ that describes dissipation and must be related to the time correlation of the noisy force via

$$H(t) = \langle \zeta(t)\zeta(0) \rangle = mk_B T K(t) \tag{3}$$

in order to be consistent with constant temperature thermodynamics conditions.

The numerical integration of this equation is a hard task, especially for the computation of the friction integral in Eq.(2), since it would require the complete storage of the past trajectory of the momenta. To overcome this problem, a Markovian linear stochastic differential equation is

introduced in an extended phase space, supplementing the physical variables with a set of n auxiliary momenta $\mathbf{s}$, linearly coupled to the physical momentum and among themselves. It has been proven that a Markovian dynamics in an extended phase-space is a practical method to simplify the treatment of non-Markovian problems.[27–29] The resulting equation can be written as:

$$\begin{pmatrix} \dot{p} \\ \dot{\mathbf{s}} \end{pmatrix} = \begin{pmatrix} -V'(x) \\ 0 \end{pmatrix} - \begin{pmatrix} a_{pp} & \mathbf{a}_p^T \\ \bar{\mathbf{a}}_p & \mathbf{A} \end{pmatrix} \begin{pmatrix} p \\ \mathbf{s} \end{pmatrix} + \begin{pmatrix} b_{pp} & \mathbf{b}_p^T \\ \bar{\mathbf{b}}_p & \mathbf{B} \end{pmatrix} \boldsymbol{\xi}. \tag{4}$$

Here, $\boldsymbol{\xi}$ is a vector of $n+1$ uncorrelated Gaussian random numbers with $\langle \xi_i(t)\xi_j(0)\rangle = \delta_{ij}\delta(t)$. All momenta are linearly coupled via the "drift matrix" $\mathbf{A}_p$ while the noise components are coupled via the "diffusion matrix" $\mathbf{B}_p$. Given the phase-space vector $\mathbf{x} = (x, p, \mathbf{s})$, it is useful to distinguish between a matrix acting on the full vector $\mathbf{x}$ and one connecting subsets of its components. Thus $\mathbf{A}_p$ and $\mathbf{B}_p$ are defined according to the notation introduced in Ref.[30] : the vectors $\mathbf{a}_p$, $\bar{\mathbf{a}}_p$, $\mathbf{b}_p$, $\bar{\mathbf{b}}_p$ represent the coupling between the p and $\mathbf{s}$ variables; a_{pp} and b_{pp} act only on the momentum p and the submatrices $\mathbf{A}$ and $\mathbf{B}$ account for the coupling between the additional momenta. Integrating out the $\mathbf{s}$ degrees of freedom in Eq.(4), a non-Markovian equation of motion for the physical variables (x, p) is recovered and it was shown[24] that the memory kernel is related to the drift and diffusion matrices via

$$K(t) = 2a_{pp}\delta(t) - \mathbf{a}_p^T e^{-|t|\mathbf{A}} \bar{\mathbf{a}}_p \tag{5}$$

as well as the noise correlation is:

$$H(t) = d_{pp}\delta(t) + \mathbf{a}_p^T e^{-|t|\mathbf{A}} \left[\mathbf{Z}\mathbf{a}_p - \mathbf{d}_p\right] \tag{6}$$

where $\mathbf{D}_p = \mathbf{B}_p\mathbf{B}_p^T$ and $\mathbf{Z} = \int_0^\infty e^{-\mathbf{A}t}\mathbf{D}e^{-\mathbf{A}^T t}dt$. The details of the integration of the auxiliary momenta $\mathbf{s}$ are reported in Ref.[24] . The elements of the matrices $\mathbf{A}_p$ and $\mathbf{B}_p$ control the memory functions of the equation, thus determining the dynamics and the stationary distribution of the system.

2.1 Pumping the system by a 'hotspot' thermostat

While it is possible to define proper conditions for Eqs.(4) to sample the canonical ensemble, *i.e.* to satisfy the fluctuation-dissipation theorem as in Eq.(3), we aim at achieving a non-equilibrium steady state for a finite time. In order to selectively excite a subset of the degrees of freedom, one has to use a GLE that does *not* satisfy the fluctuation-dissipation relation. Specifically, in this work we used a modified version of the so-called δ-thermostat,[31] which induces frequency-dependent fluctuations of the momentum of a selected range of vibrational modes, while keeping the remaining ones almost completely frozen. Our goal is to reproduce a laboratory setup where the infrared laser pumps energy into modes at a specific frequency, whereas the other degrees of freedom are not coupled directly to the laser source and remain at the equilibrium temperature. To this end a white-noise Langevin thermostat at T_{base}, characterized by a friction parameter γ_{base}, is combined with a δ-thermostat with a target temperature of T_{peak}, acting on a set of given frequencies centered around ω_{peak}.

A memory kernel whose Fourier spectrum combines a white-noise baseline and a Lorentzian shape peak can be obtained with the following parameterization for the matrices $\mathbf{A}_p$ and $\mathbf{D}_p$:

$$\mathbf{A}_p = \begin{pmatrix} \gamma_{\text{base}} & \sqrt{\frac{\gamma_{\text{peak}}\omega_{\text{peak}}}{2\pi}} & 0 \\ -\sqrt{\frac{\gamma_{\text{peak}}\omega_{\text{peak}}}{2\pi}} & \Delta\omega & \omega_{\text{peak}} \\ 0 & -\omega_{\text{peak}} & 0 \end{pmatrix} \tag{7}$$

$$\mathbf{D}_p = \begin{pmatrix} 2T_{\text{base}}\gamma_{\text{base}} & 0 & 0 \\ 0 & 2T_{\text{peak}}\Delta\omega & 0 \\ 0 & 0 & 0 \end{pmatrix}, \tag{8}$$

that gives a (friction) memory kernel whose power spectrum reads

$$K(\omega) = 2\gamma_{\text{base}} + \frac{\gamma_{\text{peak}}}{\pi} \frac{\omega_{\text{peak}}\Delta\omega\omega^2}{(\omega^2 - \omega_{\text{peak}}^2)^2 + \Delta\omega^2\omega^2}. \tag{9}$$

For small $\Delta\omega$, this kernel tends to $\delta(\omega - \omega_{\text{peak}})$. Thus, the thermostat will affect the frequencies falling in the interval $\Delta\omega$ centered around the frequency ω_{peak}, injecting energy corresponding to T_{peak}, while the white noise contribution tends to keep the other modes at the target baseline temperature T_{base}. The effect of this "hotspot" thermostat can be predicted analytically, when applied to a harmonic oscillator of frequency $\bar{\omega}$.[32] Normal modes with $\bar{\omega} \gg \omega_{\text{peak}}$ and $\bar{\omega} \ll \omega_{\text{peak}}$ equilibrate at the temperature T_{base}. A maximum in temperature is reached for $\bar{\omega} = \omega_{\text{peak}}$, which however corresponds to a different temperature than T_{peak}, due to the presence of the white-noise baseline that also interferes with the selected modes. Such maximum temperature T_{max}, for $\bar{\omega} = \omega_{\text{peak}}$, can be computed analytically, and it is thus possible to set T_{peak} to

$$T_{\text{peak}} = T_{\text{max}} - \frac{\gamma_{\text{base}} \left(T_{\text{max}} - T_{\text{peak}}\right) \left[2\pi\Delta\omega \left(\Delta\omega + \gamma_{\text{base}}\right) + \gamma_{\text{peak}}\omega_{\text{peak}}\right]}{\Delta\omega\gamma_{\text{peak}}\omega_{\text{peak}}}. \tag{10}$$

so that – in the harmonic limit – normal modes with frequency ω_{peak} equilibrate at the desired temperature T_{max}. These predictions for the behavior of a "hotspot" thermostat are qualitatively fulfilled in realistic systems, in which vibrational modes are coupled with each other by anharmonicity.

Fig. 1 shows the effect of the excitation of the OD stretching mode in deuterated methanol (left panel) and of the OH stretching mode in water (right panel) on the temperature of the D/H species. The temperature T_{base} corresponding to the other atomic species is reported as well. The details of how the kinetic temperatures reported in Fig. 1 are computed are given in the next section. In both cases we have chosen $T_{\text{max}} = 400$ K and $T_{\text{base}} = 300$ K. For both examples, after a characteristic transient time, the system reaches a steady-state, in which the species most coupled to the thermostat (D and H) have a higher kinetic energy, while the other atoms, CH_3O atoms in methanol and O atoms in water, equilibrate at $\sim T_{\text{base}}$. In the transient time after the 'hotspot' thermostat is switched on, the two systems respond in different ways. While most of the kinetic energy is effectively transferred to the modes at the target frequency, also the baseline temperature increases, due to the anharmonic coupling among different vibrational modes. In addition, the

joint action of a δ-thermostat and of a white-noise Langevin thermostat results in an effective temperature of the excited modes lower than the nominal T_{peak}.

However, T_D in methanol does not correspond exactly to the temperature of the OD stretching that is excited. Using Eq.(10) one can tune the interaction between T_{peak} and T_{base} so to achieve the desired mode temperature T_{max}. For example, in the case of methanol, with the parameters used to obtain Fig. 1, we set T_{peak} = 1460 K to obtain (in the harmonic limit) T_{max} = 400 K: the temperature of the stretching mode reported (T_{OD}) reported in Fig. S11 turns out very close the one predicted by Eq.(10) in the harmonic approximation.

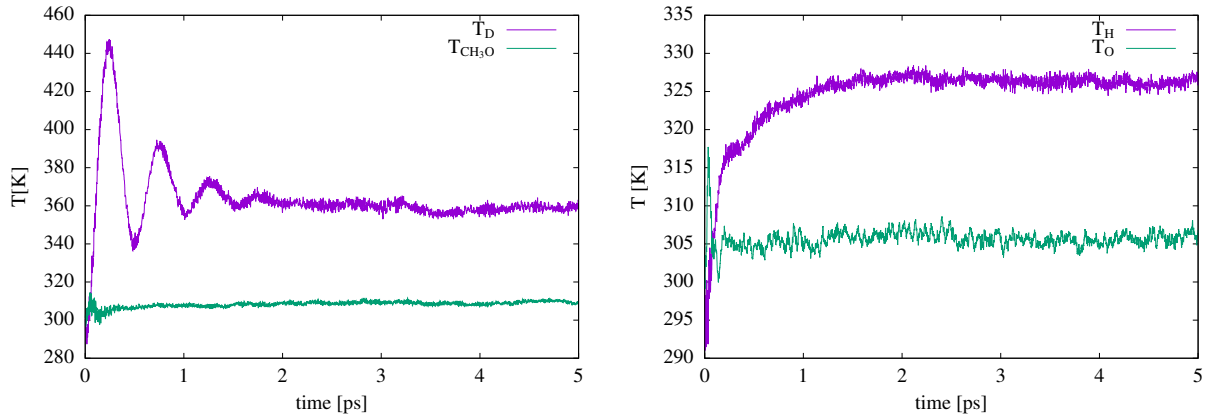

Figure 1: Kinetic temperatures during a "hotspot" thermostatting for deuterated methanol (left) and water (right). In both cases the purple (green) curve represents the temperature of the excited atoms (the remaining ones) which correspond to deuterium in left panel and hydrogen in right panel.

2.2 Probing the system relaxation

Experimentally the relaxation dynamics that follows the pump phase is probed by a second laser pulse. Vibrational spectra are collected as a function of the time delay of the probe pulse. To model the probe phase we switch off the GLE thermostat and let the system evolve in the microcanonical ensemble, so that the energy redistributes among all the degrees of freedom, to reach classical equipartition.

During relaxation the kinetic temperature of the excited modes is the most natural quantity to probe. However, further information can be obtained computing the vibrational density of states

(vDOS) from the Fourier transform of the velocity autocorrelation function. In order to reproduce the time delay between pump and probe, the NVE trajectory is divided in intervals of the same duration, during which atomic velocities are sampled and the transient vibrational spectrum is computed. This protocol allows us to probe the whole range of vibrational frequencies as a function of time, thus monitoring the real time energy diffusion between the different vibrational modes. The hotspot thermalization implies an excess energy in the selected mode, resulting in an enhanced peak intensity in the spectrum that directly reflects the population of the vibrational mode. Relaxation dynamics eventually causes the redistribution of this surplus energy and a change of the intensity of the peaks coupled to the vibrational excited mode. The computation of the time-dependent area for peaks centered at a given frequency $\bar{\omega}$

$$A(\bar{\omega}, t) = \int_{\bar{\omega}-\delta\omega}^{\bar{\omega}+\delta\omega} \left[\int_{t_1}^{t_2} \langle \mathbf{v}(t)\mathbf{v}(t+\tau) \rangle e^{-i\omega\tau} d\tau \right] d\omega \tag{11}$$

provides time-resolved quantitative information about the dynamics and the characteristic timescale of energy transfer. In what follows we always calculated vibrational spectra considering only the velocities of hydrogen or deuterium atoms, in order to better highlight the dynamics of the vibrational modes of interest.

Although the calculation of power spectra as the Fourier transform of velocity autocorrelation functions is rigorously justified only at equilibrium,[26] here we use it to probe non-equilibrium transient regimes. In the following we verify that the Green-Kubo formalism provides quantitatively reliable information about the physical properties of systems out of equilibrium, provided that the chosen time window is long enough to guarantee a suitable statistical accuracy.

3 Applications

3.1 Liquid methanol

Simulation details As a case study we consider methanol in its liquid phase. Methanol was modeled using the COMPASS force-field:[33] the presence of high-order (cubic and quartic) and cross-coupling terms provides an accurate description of intramolecular interactions. Detailed information about the force-field are given in the Supporting Information (SI). Electrostatic interactions are modeled as fixed charges, obtained by fitting the electrostatic potential of an all electron Hartree-Fock calculation performed with a medium-sized basis set 6-31G*. The fitting was performed using the RESP method.[34,35] Molecular dynamics simulations are carried out for systems of 216 CH_3OD molecules in a cubic box with periodic boundary conditions with a fixed density $\rho = 0.80$ g/cm^3. All the simulations have been performed using the LAMMPS package,[36] in which the equations of motion are integrated with a timestep of 0.5 fs. The pump-probe results are obtained by averaging over up to 128 different trajectories.

We tested the thermostat parameters over a reasonable range of values in order to address its reliability in terms of physical prediction. Each parameter for the colored contribution of the thermostat has been tested separately over the following ranges of value:

- excited mode temperature in the range $320 \leq T_{\max} \leq 600$ K;
- spectral width in the range $0.1 \leq \Delta\omega \leq 75$ cm^{-1};
- thermostat friction in the range $0.1 \leq 1/\gamma_{\text{peak}} \leq 5$ ps.

Choosing the GLE parameters within the given range ensures physically meaningful and reproducible results. No appreciable trend was observed in the physical observable as a function of such parameters, suggesting that the method is solid against the choice of different arbitrary parameters, and it reproduces the correct physics.

The convergence of the results upon the system size was also addressed. We applied the GLE protocol for systems ranging from 27 to 512 molecules. We observed that small systems are

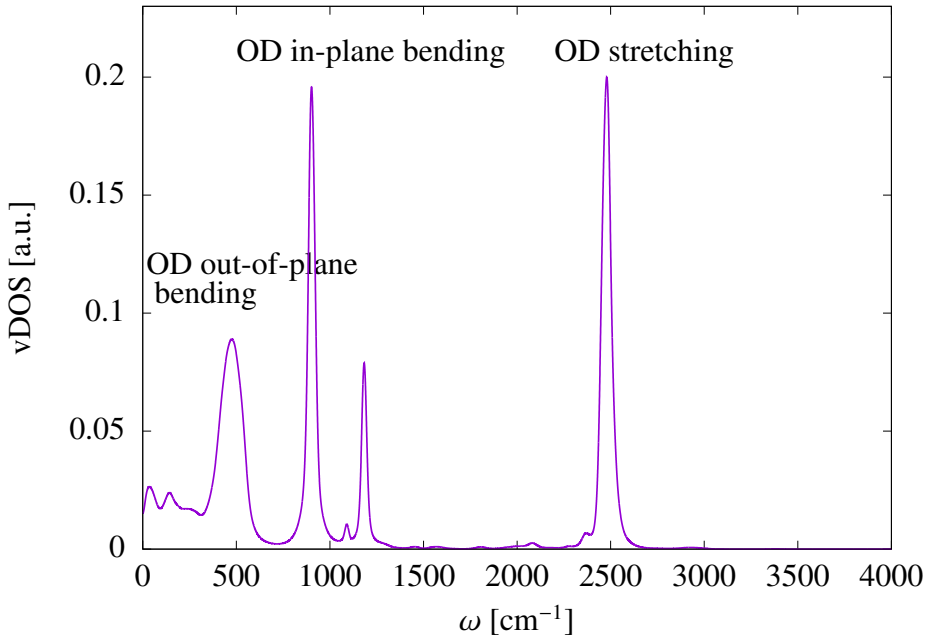

Figure 2: Vibrational density of states (vDOS) of deuterated methanol CH_3OD.

affected by finite size effects, and size convergence is reached for systems of 216 molecules or larger.

These benchmark calculations and tests are discussed in detail in the Supporting Information.

Excitation To simulate the excitation, the GLE thermostat has been applied for 5 ps in order to reach a non-equilibrium steady state. A fully anharmonic force-field results in a transient behavior of the excitation that depends on the details of the system. The dynamics of hydrogen bonded liquids is usually investigated by labeling the highest frequency vibrational mode,[3] namely: the OH stretching mode. For the sake of comparison with experimental results[37,38] we considered 100% fully deuterated methanol, CH_3OD and the excitation of the OD stretching mode.

In the equilibrium vibrational spectrum shown in Fig. 2, the frequency of the OD stretching mode is centered around $\omega_{\text{peak}} = 2477$ cm^{-1}. The power spectrum is calculated considering only deuterium velocities. Interestingly, two peaks not related to the hydroxyl group appear in the spectrum: the first one, around $\omega \sim 1080$ cm^{-1}, corresponds to the CO stretching mode, whereas

the other one, centered at $\omega \sim 1200$ cm^{-1}, is the CH_3 rocking mode. The reason for these two additional peaks can be attributed to the functional form for the bonded interactions of the force-field: in addition to the anhamornicity up to the fourth power, COMPASS provides terms for cross-interactions as, for example, a bond-bond and a bond-angle cross term. This explains how the motion of the hydroxyl group cannot be completely decoupled from the effect of other vibrational modes, which involve the surrounding bonds or angles. The vibrational spectra computed here are in good agreement with those obtained by Car-Parrinello simulations[39] as well as with experiments.[40]

The colored noise contribution of the thermostat was characterized by $T_{\text{max}} = 400$ K, $1/\gamma_{\text{peak}} = 0.5$ ps and $\Delta\omega = 1$ cm^{-1}, while the white noise Langevin part was characterized by $T_{\text{base}} = 300$ K and $1/\gamma_{\text{base}} = 0.5$ ps. Although the excitation is tuned with a narrow width, the response of the mode is broader and a small but noticeable effect on lower frequency modes can be observed (see Fig. 1). Although this feature depends on specific thermostat settings (see Supporting Information), it is the hallmark of the intrinsic coupling between the vibrational modes involving the OD bond and the other modes of the system. Furthermore, T_D is $\sim 10\%$ lower than T_{peak}. As a matter of fact T_D is a measure of the energy of all vibrational modes involving deuterium atoms, including those not affected by the thermostat. Alternatively, one can monitor the kinetic energy of the OD stretching mode, defined from the mode velocity $v_{\text{stretch}} = (\mathbf{v}_O - \mathbf{v}_D) \cdot \dfrac{\mathbf{d}_{\text{OD}}}{d_{\text{OD}}}$, where $\mathbf{d}_{\text{OD}}$ is the vector parallel to the OD bond and d_{OD} its modulus. However, we verified that the relaxation dynamics of T_D and T_{OD} has the same timescale and the results are reported in the SI.

Relaxation time The relaxation is monitored in 50 ps long NVE runs, during which atomic velocities are sampled to compute the kinetic temperature of different atomic species and the vDOS. When the GLE thermostat is switched off T_D decreases rapidly as the energy in the OD bond redistributes over the other degrees of freedom. The decay time of the temperature fits a simple exponential model

$$T_D(t) = T_D^{eq}(1 + \delta e^{-t/\tau_K}) \,, \tag{12}$$

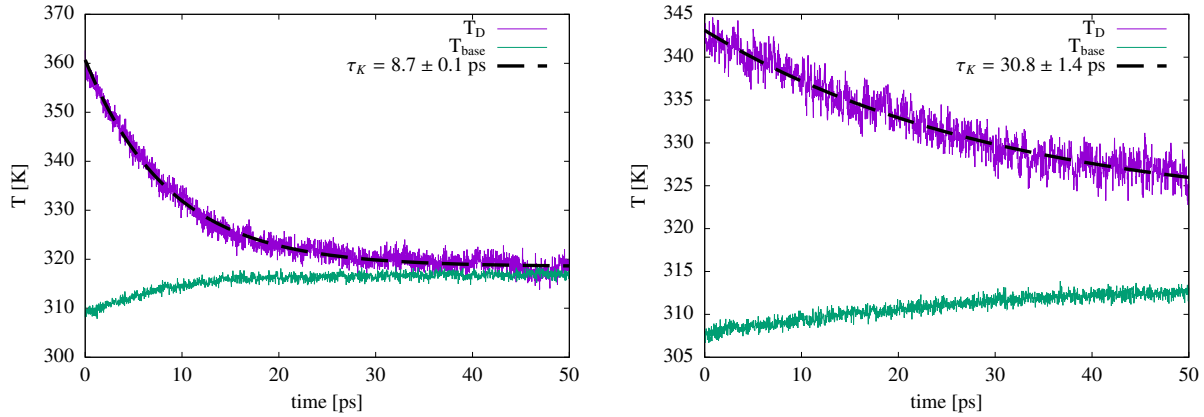

Figure 3: Kinetic temperature during the relaxation: the black dashed line is the fit obtained by means of Eq.12. Left panel shows the normal behavior of methanol, while the right panel shows the relaxation of the system when the electrostatic interactions are switched off, leaving the Lennard-Jones interactions as the sole non-bonded interactions.

where T_D^{eq} is the temperature of deuterium atoms at the end of the relaxation process (i.e. the equilibrium temperature), δ is a dimensionless factor that quantifies the excess energy at $t = 0$, and τ_K is the decay time, which turns out to be 8.7 ± 0.1 ps. The result is shown in the left panel of Fig. 3.

To assess the contribution of hydrogen bonding interactions to vibrational relaxation, we repeated the pump-probe virtual experiment switching off the electrostatic interactions. The results reported in the right panel of Fig. 3 show that the relaxation dynamics in a non-hydrogen-bonded system becomes three to four times slower, thus suggesting that energy redistribution is mainly controlled by intermolecular hydrogen bonding.

Relaxation mechanism Transient vibrational spectra are computed in time windows of 1.5 ps, spanning the relaxation trajectory each 0.5 ps: peak areas have been computed for the three main bands related to the vibrational modes involving the OD bond, namely OD stretching, in-plane bending, and out-of-plane bending modes.[40,41] The result is shown in Fig. 4, where areas, computed with Eq.(11), are reported as $A(\bar{\omega}, t) - A_{eq}(\bar{\omega})$ (where $A_{eq}(\bar{\omega})$ is the peak area at the end of the equilibrium process), for the OD stretching mode, and $A(\bar{\omega}, t) - A(\bar{\omega}, 0)$ (where $\bar{\omega}$ is the frequency of the peak and $A(\bar{\omega}, 0)$ is its area right after the excitation) for the bending modes, for a better

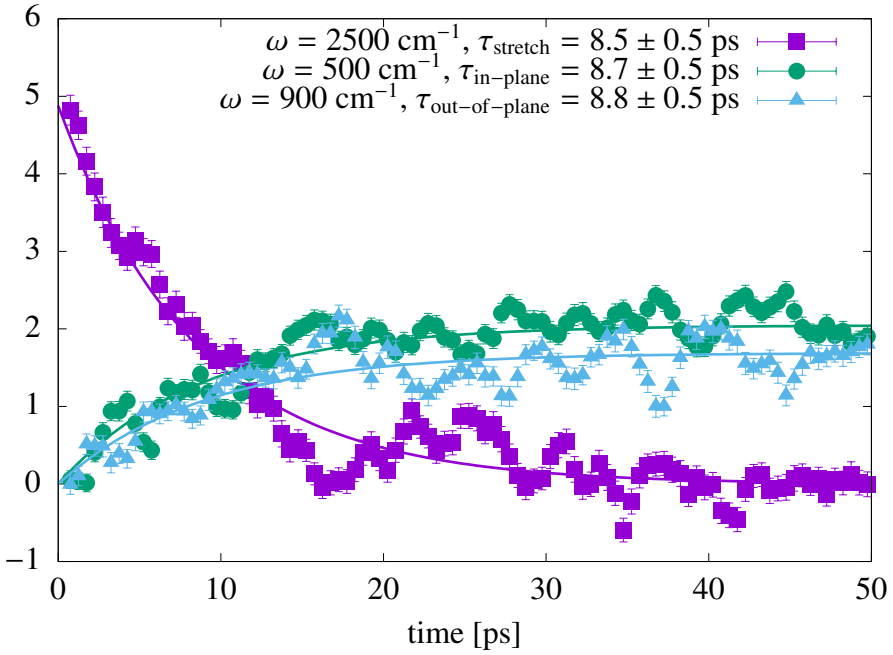

Figure 4: Peak areas as function of time as obtained from Eq.(11). In y-axis is reported relative intensity for sake of clarity: purple squares show the amount of intensity lost by stretching mode, whereas blue triangles and green circles represent the intensity gained by the bending modes. Dashed lines represent the relative fit.

comprehension. Peak intensities show an exponential trend, which is well fitted by Eq.(12), so as to obtain the characteristic timescale of these processes. The area of the excited stretching mode decreases with a lifetime of $\tau_{\text{stretch}} = 8.5 \pm 0.5$ ps, which is statistically equivalent to the decay time of the kinetic temperature T_{D}, thus crossvalidating our analysis. This is a key result, as it justifies *a posteriori* the use of time-correlation functions to calculate response functions, e.g. power spectra, from non-equilibrium trajectories. While this is a rather common practice,[17,18] it often lacks a compelling verification: extensive tests lead us to conclude that a time window of 1.5 ps is the shortest possible to achieve meaningful results, which also means that it is impossible for us to probe faster decay mechanisms by this approach.

The dimensionless pre-factor in Eq.(12) turns out to be $\delta_{\text{stretch}} = 0.37 \pm 0.01$, which means that the excitation enhances the population of the OD stretching mode by about 37% with respect to the equilibrium population. The dynamics of the low-frequency part of the spectrum shows that energy is transferred in equal amounts to the two bending modes: $\delta_{\text{in-plane}} = 0.14$ and $\delta_{\text{out-of-plane}} = 0.16$. Furthermore the calculated lifetimes show that the transferring process occurs simultaneously, $\tau_{\text{in-plane}} = 8.8 \pm 0.5$ ps and $\tau_{\text{out-of-plane}} = 8.8 \pm 0.5$ ps. The remaining energy contributes to the overall temperature increase of the system, by spreading into the remaining modes of the molecule.

3.2 Discussion

The simulation protocol described above aims at modeling pump-probe spectroscopy,[37,42] but since it is based on classical MD, substantial differences with experiments emerge, stemming from the quantum-mechanical nature of molecular vibrations. In this section we highlight analogies and differences between modeling and experiments.

The excitation-relaxation process occurring in pump-probe experiments is usually represented as a quantum-mechanical kinetic model, in which a laser pulse excites the target mode from its ground state $|0\rangle$ to its first excited state $|1\rangle$. The population of the excited state relaxes rapidly to an intermediate state $|0^*\rangle$ with a time constant τ^*. In this intermediate state, the excess vibrational

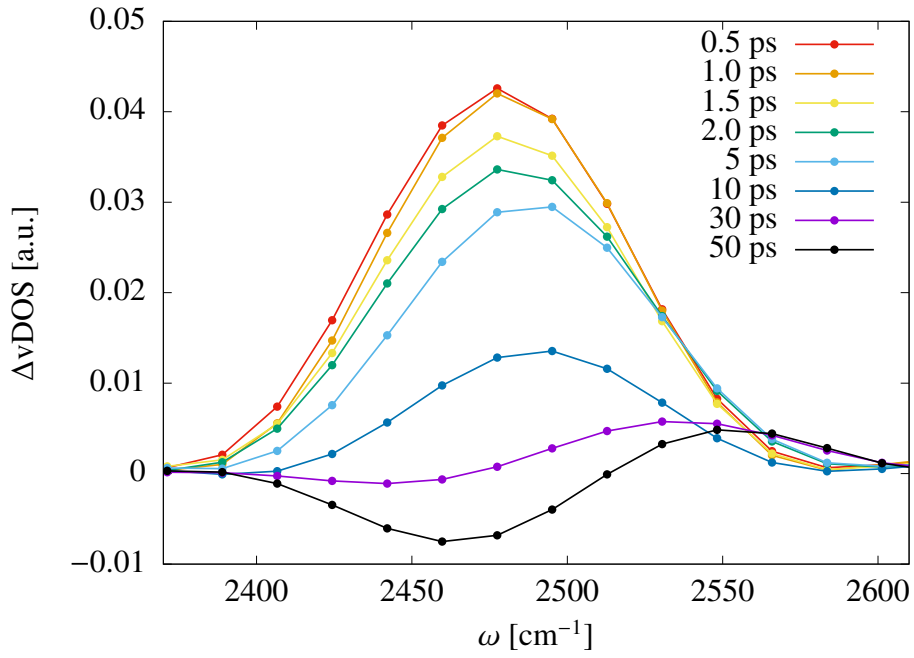

Figure 5: Amplitude difference between the non-equilibrium and the equilibrium vDOS at different times: for $t > 5$ ps peak frequency starts shifting and the final configuration ($t = 50$ ps) shows an appreciable contribution at higher frequency and a negative contribution for $2450 \leq \omega \leq 2550$ cm^{-1}, which is due to the blue shift of the OD stretching bond at higher temperatures. The amplitudes are reported as a difference with respect to a equilibrium configuration at $T = 300$ K, in order to highlight the frequency shift.

energy is not yet fully equilibrated over the system. Eventually this intermediate state relaxes to a heated ground state $|0'\rangle$ with time constant τ_{eq}, as the energy redistributes thermally among all the modes of the system. In hydrogen-bonded liquids the higher temperature of the system in the $|0'\rangle$ causes an average weakening of the hydrogen bonds, accompanied by a faster vibration of the OD stretching, i.e. a blue shift of the corresponding band.

We analyze these processes by computing the amplitude difference between the transient vDOS and the equilibrium vDOS at $T = 300$ K (Fig. 5).

The excitation from $|0\rangle$ to $|1\rangle$ is purely quantum-mechanical, and classical simulations cannot reproduce its spectral features. In fact, the quantum excitation causes a depopulation of the ground state in favor of the excited state,[43] producing an immediate change in the optical absorption spectrum, in which the intensity of the band corresponding to the excitation frequency decreases. This

effect, referred to as 'bleaching', cannot be observed in a classical molecular dynamics simulation. On the contrary, pumping 'colored' energy in an ensemble of coupled classical oscillators populates the vibrational modes at the corresponding frequency, therefore enhancing the intensity of the band in the absorption spectrum. At short timescales after the excitation ($t \leq 5$ ps) the intensity of the OD stretching band out of equilibrium is indeed higher than that at equilibrium (Fig. 5), as a consequence of the excitation of classical OD oscillators with enhanced amplitudes. At later times the differential spectra are characteristic for an equilibrated, heated liquid, with a blue-shifted OD stretching frequency: the spectra display reduced intensity at 2470 cm^{-1} (the absorption maximum before excitation) and enhanced intensity at 2550 cm^{-1}, as heated methanol molecules form weaker hydrogen-bonds (Fig 5, $t = 50$ ps).

In the experimental framework, the dynamics of the two relaxations occurs over different timescales: the excited state is short-lived and is characterized by a sub-picosecond lifetime; on the other hand the intermediate state relaxes with a longer time constant. Here we address the vibrational energy redistribution that occurs over longer timescales, as our setup and analysis tools are not suitable to investigate $\tau < 1$ ps. We remark that sub-picosecond processes have been investigated in previous theoretical papers for water,[16–18] while, to the best of our knowledge, methanol relaxation has not been studied theoretically. Whereas the differences in the excitation mechanism between experiments and simulations may affect the fast relaxation dynamics from $|1\rangle$ to $|0^*\rangle$, the subsequent thermal energy relaxation from $|0^*\rangle$ to $|0'\rangle$ is essentially classical and can be probed by molecular dynamics. The timescale calculated for the relaxation of deuterated methanol, 8.5 ps, agrees well with the experimental thermal relaxation time $\tau_{eq} \sim 6.0, 7.0$ ps in Ref.[37,42] The small difference may be ascribed to the approximate classical forcefield.

Such agreement suggests that the underlying relaxation processes at the molecular level unraveled by our simulations are similar to the thermalization that occurs after the depopulation of the excited state of the (quantum) oscillator in experiments. Thus, even though simulated transient spectra show unlike signatures of classical excitations as compared to experiments,[37] the good agreement in the timescales ruling the observed phenomena indicates that the simulation accounts

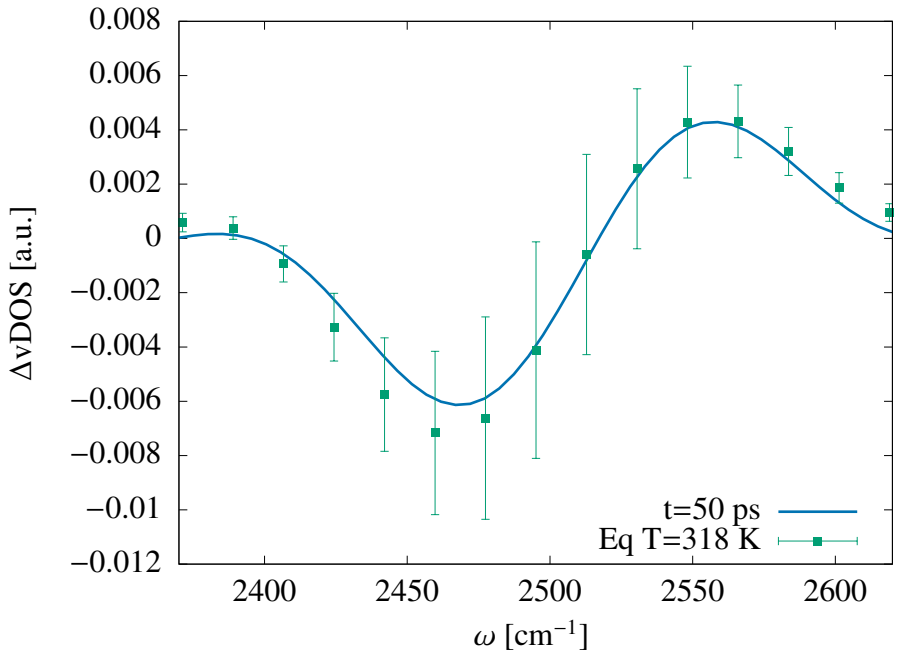

Figure 6: Comparison between the spectrum relative to the final configuration ($t = 50$ ps) and the equilibrium vDOS computed at $T = 318$ K. The amplitudes are reported as a difference with respect to a equilibrium configuration at $T = 300$ K, in order to highlight the thermal induced blue shift.

for the correct mechanism and rate limiting step of the experimentally observed thermalization dynamics.

By the end of the relaxation, i.e. after 30 ps, the whole energy pumped into the OD stretching is converted into thermal energy. Specifically, with the parameters chosen for the excitation discussed in the previous section, the temperature of the system increases from 300 K to 318 K. The blue shift observed at the end of the relaxation is thermal, as it is suggested by the agreement between the transient spectrum taken at $t = 50$ ps and the vDOS computed at equilibrium for $T = 318$ K (Fig. 6),

Furthermore the behavior of the bending modes confirms that the system state at $t = 0$ corresponds to the intermediate state $|0^*\rangle$, in which the vibrational ground state of the stretching mode is coupled with lower frequency modes[44,45] determining the main channel for energy redistribution. Interestingly, this relaxation mechanism is independent on the isotopic dilution of the mixture:

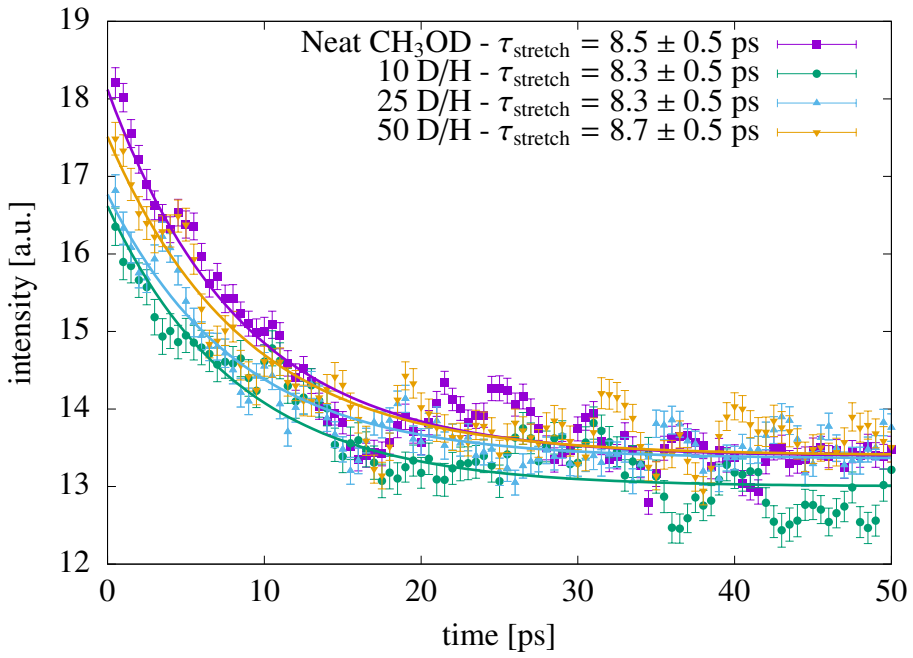

Figure 7: Comparison between systems with different isotopic dilution, namely the 10%, 25% and 50% of deuterated molecules. Different intensities correspond to different populations of OD oscillators, but the relaxation timescales are independent on dilution.

the same dynamics is observed for different isotopic dilution, 10%, 25% and 50% of deuterated molecules, as showed by Fig. 7. Different peak intensities at $t = 0$ correspond to different mode populations, which depend on the number of oscillators in the system. This is in agreement with previous experimental results,[37] showing that the relaxation from the intermediate state does not depend on the isotopic composition of the system. The dependence on the isotopic dilution of the fast relaxation time, instead, is still debated.[37,38,42]

4 Liquid water

The second case study is liquid water. While still a hydrogen bonded liquid, its dynamics is considerably different from that of methanol, since each molecule forms more hydrogen bonds.[46,47]

In this work liquid water is modeled via a force-field fitted to first-principles MD simulations by force-matching.[48] This force-field has shown to accurately reproduce the structural and dynamical

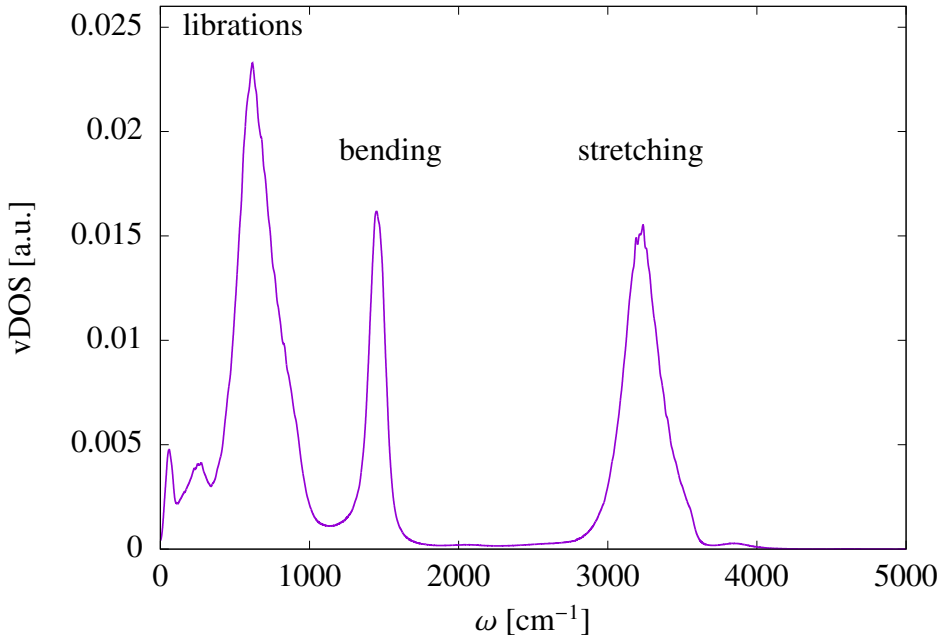

Figure 8: Vibrational density of states (vDOS) of water calculated from the hydrogen atoms velocity autocorrelation function: the three bands of interest are the OH stretching, a broad band centered at about 3250 cm^{-1}, the bending ($\sim$ 1450 cm^{-1}) and the librations ($\sim$ 650 cm^{-1}).

properties of water simulated by density functional theory using the generalized gradient functional by Perdew, Burke and Ernzerhof.[49] Simulations have been performed on a system of 343 molecules in a periodically repeated cell with a density of $\rho = 1.0$ g/cm^3, averaging over 256 statistically independent trajectories. We adopted the same GLE thermostat settings as in the methanol case: the colored excitation was characterized by $T_{\mathrm{mas}} = 400$ K, $1/\gamma_{\mathrm{peak}} = 0.5$ ps and $\Delta\omega = 1$ cm^{-1}, while the white noise Langevin has $T_{\mathrm{base}} = 300$ K and $1/\gamma_{\mathrm{base}} = 0.5$ ps. Here we focus on the OH stretching mode which, gives a broad vibrational band centered at 3211 cm^{-1}, as shown by the vDOS in Figure 8.

After a 5 ps-long excitation, the system relaxation was monitored for 30 ps. As mentioned above, the response of water to the thermostat shows a noticeable difference with respect to methanol (Fig. 1): frequency-dependent thermalization reaches the steady state in a few hundreds timestep. This difference is attributed to the relatively larger number of degrees of freedom involved in the excitation, compared to methanol. Since the thermostat forces the excitation over

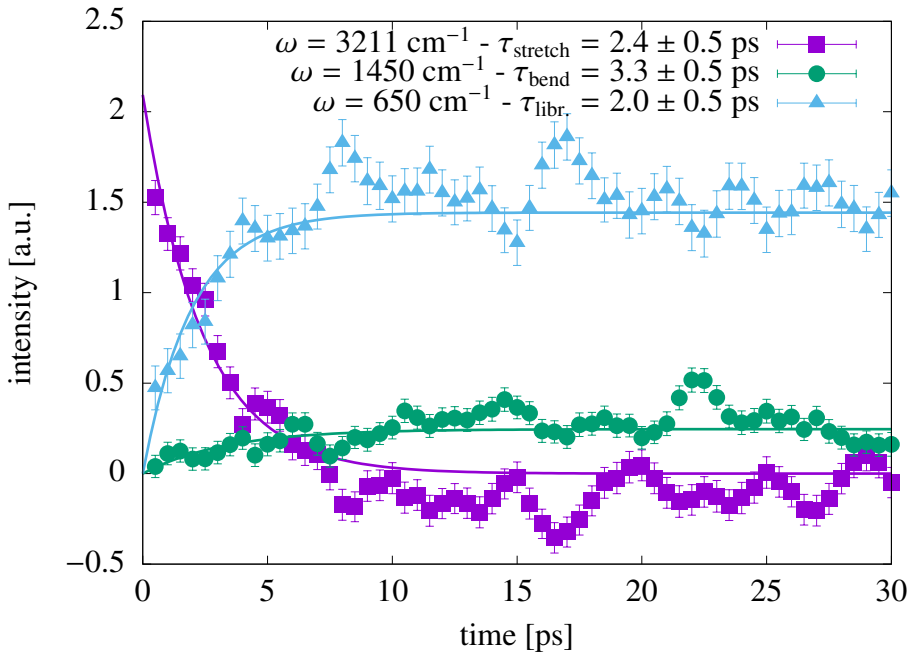

Figure 9: Peak areas as function of time as obtained from Eq.(11). In y-axis is reported relative intensity. Dashed lines represent the relative fit.

an oscillator surrounded by a number of other oscillators damped by γ_{base}, the difference in the relative number of degrees of freedom affects the transient regime prior to the steady state.

The analysis of the transient power spectra highlights further differences between water and methanol. As shown in Fig. 9 the decay of the excited OH stretching vibration occurs on a faster timescale with $\tau_{\text{stretch}} = 2.4 \pm 0.5$ ps, which is slower than the experimentally observed equilibration time of 0.7ps.[12] The slower relaxation observed in simulations may be related to additional relaxation channels, such as Fermi-resonances,[50] which classical simulations cannot account for. Notably, τ_{stretch} is significantly faster for water than for methanol. This difference may be traced back to the fact that water molecules form from 3 to 4 hydrogen bonds,[51] while methanol has only 2. Hence, stronger coupling among water molecules and higher connectivity of the hydrogen bonds network provide more channels for vibrational relaxation, leading to shorter relaxation times. Also the relaxation mechanism is different from that of methanol. Fig. 9 reports the intensity of the accepting modes, where librations are preferred with respect to bending modes. In fact, the pre-factors in the fitting equation (12) result in $\delta_{\text{stretch}} = 0.16 \pm 0.01$, $\delta_{\text{bend}} = 0.021 \pm 0.009$

and $\delta_{\text{libr.}} = 0.08 \pm 0.01$, which indicates that most of the energy relaxes into librational modes.

In addition, in water the amount of excess energy that is converted into heat is noticeably larger, thus explaining the higher temperature increase. This energy relaxation timescale of 2.5 ps compares well with experiments that show diffusive rotations in water to occur in $\lesssim 3$ ps.[52,53] The dynamics of these low frequency modes associates with collective reorientation of the HB network, and the time scale is in agreement with the diffusive rotational dynamics of water.

5 Conclusions

In summary, we have shown that, by properly designing its memory kernel, GLE can be used to selectively excite a narrow range of frequencies of a system at room temperature, leaving the other degrees of freedom almost unperturbed. The "hotspot" thermostat is suitable to model the excitation phase in a pump-probe IR experiment by MD, within the limitations imposed by the classical character of MD. Once the thermostat is switched off one can study the relaxation dynamics of condensed phase systems over the ps timescale. We have applied this approach to two hydrogen-bonded liquids, methanol and water, proving that the relaxation dynamics is independent on the parameters of the excitation. We provided an in-depth investigation of two different systems, liquid methanol and liquid water, performing a systematic analysis on the technical features of the method. The hotspot thermostat has proved to be reliable yielding robust results while adopting a broad range of settings, in particular showing that the relaxation mechanism is independent on the T_{peak}, which recalls the fact that a sample dynamics does not depend on the laser intensity.[42] We believe that this approach can be used to investigate vibrational relaxation on several systems, even more complex than those studied in this work.

Given that the GLE can be applied straightforwardly to any form of interatomic potential, and that the results are robust to considerable changes of the parameters, an application to ab initio molecular dynamics constitutes a natural extension of this work.

Acknowledgement

R.D. acknowledges Regione Sardegna for financial support under Project P.O.R.Sardegna F.S.E. 2007-2013 (Axis IV Human Resources, Objective l.3, Line of Activity l.3.1.). M.C. acknowledges funding from the Swiss National Science Foundation (project ID 200021-159896)

Supporting Information Available

Systematic testing of the parameters of the “hotspot" thermostat, size convergence tests, kinetic temperature of the excited degrees of freedom, and details about the forcefield used for methanol. This material is available free of charge via the Internet at `http://pubs.acs.org/`.

References

(1) Fecko, C. J.; Eaves, J. D.; Loparo, J. J.; Tokmakoff, A.; Geissler, P. L. Ultrafast Hydrogen-Bond Dynamics in the Infrared Spectroscopy of Water. *Science* **2003**, *301*, 1698–1702.

(2) Josefssonm, I.; Eriksson, S. K.; Ottosson, N.; G.Öhrwall,; Siegbahn, H.; Hagfeldt, A.; Rensmo, H.; Odelius, O. B. M. Collective hydrogen-bond dynamics dictates the electronic structure of aqueous I3-. *Phys. Chem. Chem. Phys.* **2013**, *15*, 20189–20196.

(3) Bakker, H. J.; Skinner, J. L. Vibrational Spectroscopy as a Probe of Structure and Dynamics in Liquid Water. *Chem. Rev.* **2010**, *110*, 1498–1517.

(4) Laenen, R.; Gale, G. M.; Lascoux, N. IR Spectroscopy of Hydrogen-Bonded Methanol: Vibrational and Structural Relaxation on the Femtosecond Time Scale. *J. Phys. Chem. A* **1999**, *103*, 10708–10712.

(5) Vodopyanov, K. L. Saturation studies of H20 and HDO near 3400 cm-1 using intense picosecond laser pulses. *J. Chem. Phys.* **1991**, *94*, 5389–5393.

(6) Luzar, A.; Chandler, D. Hydrogen-bond kinetics in liquid water. *Nature* **1996**, *379*, 55–57.

(7) Lawrence, C. P.; Skinner, J. L. Vibrational spectroscopy of HOD in liquid D2O. III. Spectral diffusion, and hydrogen-bonding and rotational dynamics. *J. Chem. Phys.* **2003**, *118*, 264–272.

(8) Ohno, K.; Okimura, M.; Akaib, N.; Katsumoto, Y. The effect of cooperative hydrogen bonding on the OH stretching-band shift for water clusters studied by matrix-isolation infrared spectroscopy and density functional theory. *Phys. Chem. Chem. Phys.* **2005**, *7*, 3005–3014.

(9) Li, F.; Skinner, J. L. Infrared and Raman line shapes for ice Ih. II. H2O and D2O. *J. Chem. Phys.* **2010**, *133*, 244504.

(10) Shi, L.; Gruenbaum, S. M.; Skinner, J. L. Interpretation of IR and Raman Line Shapes for H2O and D2O Ice Ih. *J. Phys. Chem. B* **2012**, *116*, 13821–13830.

(11) Cowan, M. L.; Bruner, B. D.; Huse, N.; Dwyer, J. R.; Chugh, B.; Nibbering, E. T. J.; Elsaesser, T.; Miller, R. J. D. Ultrafast memory loss and energy redistribution in the hydrogen bond network of liquid H2O. *Nature* **2005**, *434*, 199–202.

(12) Ramasesha, K.; Marco, L. D.; Mandal, A.; Tokmakoff, A. Water vibrations have strongly mixed intra- and intermolecular character. *Nat. Chem.* **2013**, *5*, 935–940.

(13) van der Post, S. T.; Bakker, H. J. Femtosecond Mid-Infrared Study of the Reorientation of Weakly Hydrogen-Bonded Water Molecules. *J. Phys. Chem. B* **2014**, *8*, 8179–8189.

(14) Vartia, A. A.; Mitchell-Koch, K. R.; Stirnemann, G.; Laage, D.; Thompson, W. H. On the Reorientation and Hydrogen-Bond Dynamics of Alcohols. *J. Phys. Chem. B* **2011**, *115*, 12173–12178.

(15) Długosz, M.; Antosiewicz, J. M. Evaluation of Proteins Rotational Diffusion Coefficients from Simulations of Their Free Brownian Motion in Volume-Occupied Environments. *J. Chem. Theory Comput.* **2014**, *10*, 481–491.

(16) Nagata, Y.; Yoshimune, S.; Hsieh, C.; Hunger, J.; Bonn, M. Ultrafast Vibrational Dynamics of Water Disentangled by Reverse Nonequilibrium Ab Initio Molecular Dynamics Simulations. *Phys. Rev. X* **2015**, *5*, 021002.

(17) Yagasaki, T.; Saito, S. A novel method for analyzing energy relaxation in condensed phases using nonequilibrium molecular dynamics simulations: Application to the energy relaxation of intermolecular motions in liquid water. *J. Chem. Phys.* **2011**, *134*, 184503.

(18) Yagasaki, T.; Ono, J.; Saito, S. Ultrafast energy relaxation and anisotropy decay of the librational motion in liquid water: A molecular dynamics study. *J. Chem. Phys.* **2009**, *131*, 164511.

(19) Hasegawa, T.; Tanimura, Y. Calculating fifth-order Raman signals for various molecular liquids by equilibrium and nonequilibrium hybrid molecular dynamics simulation algorithm. *J. Chem. Phys.* **2006**, *125*, 074512.

(20) Hasegawa, T.; Tanimura, Y. Nonequilibrium molecular dynamics simulations with a backward-forward trajectories sampling for multidimensional infrared spectroscopy of molecular vibrational modes. *J. Chem. Phys.* **2006**, *128*, 064511.

(21) Ito, H.; Tanimura, Y. Simulating two-dimensional infrared-Raman and Raman spectroscopies for intermolecular and intramolecular modes of liquid water. *J. Chem. Phys.* **2016**, *144*, 074201.

(22) King-Smith, R. D.; Vanderbilt, D. Theory of polarization of crystalline solids. *Phys. Rev. B* **1993**, *47*, 1651–1654.

(23) Skinner, J. L.; Park, K. Calculating Vibrational Energy Relaxation Rates from Classical Molecular Dynamics Simulations: Quantum Correction Factors for Processes Involving Vibration-Vibration Energy Transfer. *J. Phys. Chem. B* **2001**, *105*, 6716–6721.

(24) Ceriotti, M.; Bussi, G.; Parrinello, M. Colored-Noise Thermostats à la Carte. *J. Chem. Theory Comput.* **2010**, *6*, 1170–1180.

(25) Ceriotti, M.; Bussi, G.; Parrinello, M. Langevin Equation with Colored Noise for Constant-Temperature Molecular Dynamics Simulations. *Phys. Rev. Lett.* **2009**, *102*, 020601.

(26) Zwanzig, R. *Non-equilibrium Statistical Mechanics*; Oxford University Press: 198 Madison Avenue, New York, New York 10016, 2001; pp 18–21.

(27) Marchesoni, F.; Grigolini, P. On the extension of the Kramers theory of chemical relaxation to the case of nonwhite noise. *J. Chem. Phys.* **1983**, *78*, 6287.

(28) Łuczka, J. Non-Markovian stochastic processes: Colored noise. *Chaos* **2005**, *15*, 026107.

(29) Mori, H. A Continued-Fraction Representation of the Time-Correlation Functions. *Prog. Theor. Phys.* **1965**, *34*, 399–416.

(30) Ceriotti, M.; Bussi, G.; Parrinello, M. Nuclear quantum effects in solids using a colored-noise thermostat. *Phys. Rev. Lett.* **2009**, *103*, 030603.

(31) Ceriotti, M.; Parrinello, M. The δ-thermostat: selective normal-modes excitation by colored-noise Langevin Dynamics. *Procedia Computer Sci.* **2010**, *1*, 1607–1614.

(32) Ceriotti, M. A novel framework for enhanced molecular dynamics based on the generalized Langevin equation. Ph.D. thesis, ETH Zürich, 2010.

(33) Sun, H. COMPASS: An ab Initio Force-Field Optimized for Condensed-Phase Applications Overview with Details on Alkane and Benzene Compounds. *J. Phys. Chem. B* **1998**, *102*, 7338–7364.

(34) Bayly, C. I.; Cieplak, P.; Cornell, W. D.; Kollman, P. A. A Well-Behaved Electrostatic Potential Based Method Using Charge Restraints For Determining Atom-Centered Charges: The RESP Model. *J. Chem. Phys.* **1993**, *97*, 10269–10280.

(35) Cornell, W. D.; Cieplak, P.; Bayly, C. I.; Kollman, P. A. Application of RESP charges to calculate conformational energies, hydrogen bond energies, and free energies of solvation. *J. Am. Chem. Soc.* **1993**, *115*, 9620–9631.

(36) Plimpton, S. J. Fast Parallel Algorithms for Short-Range Molecular Dynamics. *J. Comput. Phys.* **1995**, *117*, 1–19.

(37) Mazur, K.; Bonn, M.; Hunger, J. Hydrogen Bond Dynamics in Primary Alcohols: A Femtosecond Infrared Study. *J. Phys. Chem. B* **2015**, *119*, 1558–1566.

(38) Shaw, D. J.; Panman, M. R.; Woutersen, S. Evidence for Cooperative Vibrational Relaxation of the NH-, OH-, and OD-Stretching Modes in Hydrogen-Bonded Liquids Using Infrared Pump-Probe Spectroscopy. *Phys. Rev. Lett.* **2009**, *103*, 227401.

(39) Pagliai, M.; Cardini, G.; Righini, R.; Schettino, V. Hydrogen bond dynamics in liquid methanol. *J. Chem. Phys.* **2003**, *119*.

(40) Falk, M.; Whalley, E. Infrared Spectra of Methanol and Deuterated Methanols in Gas, Liquid and Solid Phases. *J. Chem. Phys.* **1961**, *34*, 1554–1568.

(41) Tanaka, C.; Kuratani, K.; Mizushima, S. In-plane normal vibrations of methanol. *Spectrochim. Acta* **1957**, *9*, 265–269.

(42) Lock, A. J.; Woutersen, S.; Bakker, H. J. Ultrafast Energy Equilibration in Hydrogen-Bonded Liquids. *J. Phys. Chem. A* **2001**, *105*, 1238–1243.

(43) Rezus, Y. L. A.; Bakker, H. J. On the orientational relaxation of HDO in liquid water. *J. Chem. Phys.* **2005**, *123*, 114502.

(44) Finzi, J.; Hovis, F. E.; Panfilov, V. N.; Hess, P.; Moore, C. B. Vibrational relaxation of water vapor. *J. Chem. Phys.* **1977**, *67*, 4057–4061.

(45) Nienhuys, H.; Woutersen, S.; van Santen, R. A.; Bakker, H. J. Mechanism for vibrational relaxation in water investigated by femtosecond infrared spectroscopy. *J. Chem. Phys.* **1999**, *111*, 1494–1500.

(46) Wernet, P.; Nordlund, D.; Bergmann, U.; M. Cavalleri, M. O.; Ogasawara, H.; Näslund, L. . A.; Ojamäe, T. K. H. L.; Glatzel, P.; Pettersson, L. G. M.; Nilsson, A. The Structure of the First Coordination Shell in Liquid Water. *Science* **2004**, *304*, 995–999.

(47) Smith, J. D.; Cappa, C. D.; Wilson, K. R.; Messer, B. M.; Cohen, R. C.; Saykally, R. J. Energetics of Hydrogen Bond Network Rearrangements in Liquid Water. *Science* **2004**, *306*, 851–853.

(48) Fritsch, S.; Potestio, R.; Donadio, D.; Kremer, K. Nuclear Quantum Effects in Water: A Multiscale Study. *J. Chem. Theory Comput.* **2014**, *10*, 816–824.

(49) Perdew, J. P.; Burke, K.; Ernzerhof, M. Generalized Gradient Approximation Made Simple [Phys. Rev. Lett. 77, 3865 (1996)]. *Phys. Rev. Lett.* **1997**, *78*, 1396–1396.

(50) van der Post, S. T.; Hsieh, C.-S.; Okuno, M.; Nagata, Y.; Bakker, H. J.; Bonn, M.; Hunger, J. Strong frequency dependence of vibrational relaxation in bulk and surface water reveals sub-picosecond structural heterogeneity. *Nat. Commun.* **2015**, *6*, 8384.

(51) Lin, I. C.; Seitsonen, A. P.; Tavernelli, I.; Rothlisberger, U. Structure and Dynamics of Liquid Water from ab Initio Molecular Dynamics-Comparison of BLYP, PBE, and revPBE Density Functionals with and without van der Waals Corrections. *J. Chem. Theory Comput.* **2012**, *8*, 3902–3910.

(52) Nienhuys, H.; van Santen, R. A.; Bakker, H. J. Orientational relaxation of liquid water molecules as an activated process. *J. Chem. Phys.* **2000**, *112*, 8487–8494.

(53) Laenen, R.; Rauscher, C.; Laubereau, A. Local Substructures of Water Studied by Tran-

sient Hole-Burning Spectroscopy in the Infrared: Dynamics and Temperature Dependence. *J. Phys. Chem. B* **1998**, *102*, 9304–9311.

Graphical TOC Entry